HOSTED BY
ELSEVIER
CrossMark
Available online at www.sciencedirect.com
ScienceDirect
Biosurface and Biotribology 2 (2016) 49–58
www.elsevier.com/locate/bsbt

Experiment study on puncture force between MIS suture needle and soft tissue

X. Bao[a], W. Li[a,*], M. Lu[b], Z.R. Zhou[a]

[a]*Tribology Research Institute, Key Laboratory for Advanced Technology of Materials of Ministry of Education, Southwest Jiaotong University, Chengdu 610031, China*
[b]*Department of Ultrasound, Sichuan Academy of Medical Sciences & Sichuan Province People's Hospital, Chengdu 610072, China*

Received 4 May 2016; accepted 19 May 2016

Abstract

In this paper, the interactive action between minimally invasive surgical suture needle and soft tissue was investigated under different insertion velocities, needle geometries, insertion angles and tissue characteristics to simulate the real surgical suture needle-tissue operation conditions. Experimental results demonstrated that the process of insertion was divided into two phases: no break phase and break phase. The puncture force generated at the mutation point where the tissue surface was breached. The puncture force and time for the first puncture significantly decreased with the increasing insertion velocity. The needle with triangle cross-section tip and larger size showed higher puncture force than that with round cross-section and smaller one. The penetration force reduced evidently with the advancing insertion angle, and it reached the lowest value when the angle is 90°. Moreover, an empirical single-parameter model of third-degree polynomial could predict the stiffness when a suture needle inserted into a complex soft tissue and showed a good fit to the experiment data. The results would provide reliable and significant mechanical database for the design of force feedback system in the surgical suture, either in endoscopic surgery or robotic suturing.

Keywords: Surgical suture needle; Soft tissue; Puncture force; Interaction model; Insertion velocity; Insertion angle

1. Introduction

Suturing is a ubiquitous element in minimally invasive surgery (MIS), such as endoscopic or laparoscopic operation, which is less traumatic to patients and executes better post-operative recovery. Suturing remains, however, a meticulous, time-consuming and complex task [1,2]. In addition, for the complement of an automated suture, the robot should identify the types of forces that a needle experiences during a typical suture. Thus, in order to enhance suturing efficiency and clarify suturing procedure, the specific interaction mechanism between suture needle and human organ required to be investigated. After a comprehensive review of abundant literature, it finally confirmed that studies on the mechanical characteristics between MIS suture needle and living tissue were rarely to be found. Nevertheless, there are studies in profusion on the needle-tissue interaction in the fields of biopsies and therapeutic application, it can be taken as reference for the following research.

Okamura et al. [3] chose bovine liver as the sample material and held the view that the force applied by the tissue was composed by three parts: stiffness forces before the break occurring, frictional forces and cutting forces. And then, he took a silicone rubber phantom and studied the effects of needle geometry on the total force, and proved the larger the diameter, the higher the insertion force required. Podder et al. [4] made a statistical model to estimate the maximum force that the needle would undergo in the process of insertion into the perineum and the prostate. DiMaio and Salcudean [5] measured the force profile along the needle during penetration into a phantom of PVC. They identified a force model with a peak at the needle tip, following a constant shaft force density. Crouch et al. [6] recommended a velocity-dependent needle shaft force density model. A force–displacement curve was obtained from the insertion into a silicone gel phantom of the needle. Mahvash and

*Corresponding author.
E-mail address: liweijiani@home.swjtu.edu.cn (W. Li).
Peer review under responsibility of Southwest Jiaotong University.

http://dx.doi.org/10.1016/j.bsbt.2016.05.001

Dupont [7] inserted a 19 G diamond tip needle into a porcine heart tissue at speeds of a wide range from 1 mm/s to 100 mm/s and concluded that the force decreased with the increasing speed at the moment of puncture. Mahvash and Dupont [8] identified the speeding up of needle insertion will roughly reduce the stiffness force. Chentanez et al. [9] have modeled the tissue deformation of the prostate gland with a straight hollow needle. Misra et al. [10] hold that a vital amount of force is concentrated at the pinpoint, which means it is significant to model the prick event the tissue undergoes.

Nevertheless, the most differentiation is the needle used in the former studies are generally straight and soft, while the aim of the paper is to analyze the interaction forces experienced when a rigid curved needle is insertion into living tissue samples. A systematic examination has been conducted with numerous variables, including insertion velocities, insertion angles, tissue materials and needle types.

In this paper, the main detail is organized as follows: Section 2 is devoted to recommending the materials and experiment apparatus, Section 3 models the needle-tissue interaction with a simple polynomial and presented the experiment result. Section 4 is a conclusion and dedicated to decipher and discuss the result from the experiment.

2. Materials and methods

2.1. Materials

Liver trauma is the most common and serious in abdominal trauma, the timely suturing on the liver is particularly important. Besides, liver is one of the solid organs with more relative homogeneous structure than other tissues in abdominal cavity, furthermore, porcine liver has the analogous bio-mechanical characteristics and morphological structure with human's [11]. Consequently, porcine was chosen as an experimental sample for this study, as shown in Fig. 1(a). Several excised fresh porcine livers were prepared for the study. The models separated from pigs were transported to laboratory within 1 h postmortem, the pigs were 15–22 weeks old, and they weighed 100 ± 5 kg. To avoid dehydration, the porcine liver samples were cut into $130 \times 60 \times 15$ mm^3 rectangular solid and tested within 4 h after extraction. The surface topography of the liver sample were observed by an asana microscope (SZX16, OLYMPUS, JAPAN).

In order to investigate the effect of various tissue characteristics on the insertion force during the insertion, the fresh samples of porcine skin, rabbit liver, rabbit small and large intestine were used, which were provided by animal experimental center. And the sizes of the above samples was about $100 \times 60 \times 1$ mm^3, $40 \times 30 \times 15$ mm^3, $100 \times 10 \times 0.5$ mm^3 and $100 \times 20 \times 0.5$ mm^3, respectively. All the samples were tested within 4 h after extraction.

All specimens were prepared and tested at a nominal room temperature of 20 ± 2 °C and relative humidity of $60 \pm 6\%$. During all the tests, the physiological saline were sprayed on the surface of the tissue samples every 20 min to simulate their surface moisture in the body.

The suture needle samples in this study were MIS suture needle used for clinic, which contained the following four common types: Δ1/2 10 × 28, O1/2 10 × 28, Δ1/2 8 × 20 and O1/2 8 × 20, Δ and O refer to the cross-section shape of the needle tip, which is triangular and circular respectively. 1/2 means the body of needle was crooked in semicircle, 8 and 10 refer to needle's diameter, 20 and 28 is the chord length of the curved needle, as shown in Fig. 1(b). The needles were embedded into a rectangular matrix, which is the mixture of base polymers and base resin (Fig. 1(c)). All rims of the matrix were burnished smooth, which is benefit to grasp

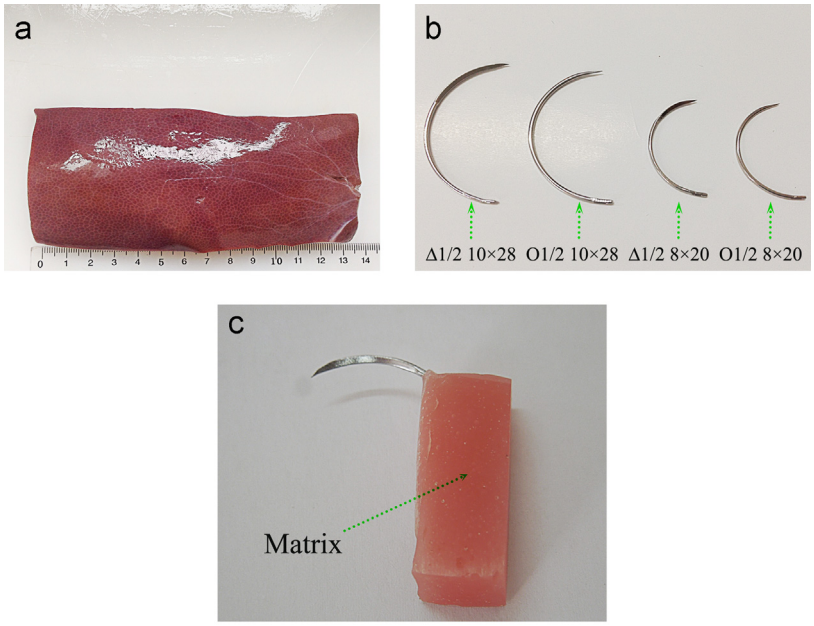

Fig. 1. Experimental samples, (a) Excised fresh porcine liver sample ($130 \times 60 \times 15$ mm^3), (b) Four types of suture needles: Δ1/2 10 × 28, O1/2 10 × 28, Δ1/2 8 × 20 and O1/2 8 × 20, (c) An embedded needle installed in the clamps of the testing machine.

symmetrically and solidly in the clips of the bio-mechanical testing machine.

2.2. Experiment apparatus and data collection

The bio-mechanical tests relate to needle insertion were conducted in a 1-DOF electronic universal material testing machine (HY0580, Shanghai Hengyi Testing Machine Co., Ltd., China), which was commonly used for operating the bio-mechanical tests of biological tissues, such as tensile, compression, acupuncture, stripping trial et al., as depicted in Fig. 2. The actuator of the testing machine was equipped with a 6-DOF force transducer (Transcell Technology Inc., America) and installed at the end of the folder. It can test the total interaction force originating from the needle insertion into tissue. The force sensor's resolution is less than 0.01% and its testing range is larger than 1 mN but less than 50 N, the displacement accuracy is $<0.2\%$ and the maximum movement is up to 800 mm. The actuating device was an alternating-current servo motor (Panasonic MINAS A4 SERIES Corp., Japan). The insertion velocities we can chose in the present study are from 0.001 mm/min to 500 mm/min. The testing machine is controlled by a microcomputer and the sampling rates we set here is 50 Hz. The biological tissues were placed in a right position just below the fixture which was used for clamping the suture needle solidly in the piercing process. The data and curves would be automatically recorded by the microcomputer control system. Re-productively test were performed under the same testing parameters. Each test was operated on different parts of the same porcine liver, and the spaces between every two insertion points were generally uniform. They were approximately 2 mm and long enough to preclude the interference caused by previous insertion and prevent the needle from following an existing path.

2.3. Analysis of interactions model

In this part, the stiffness force is put forward, which is only exerted by the needle before a puncture happens. The stiffness force is resulted by the viscoelasticity of tissue. Several different linear (relatively for small deflection) [12] and non-linear (for large deformation) [5,13] models relate to needle insertion have been investigated. Cubic polynomial is taken to develop models by the no-linear least squares algorithm, which can obtain the polynomial coefficient. What draws attention is, because the tissue is preconditioned in the testing platform, the model developed from experiment would not exactly coincide with the data from actual clinical operation.

The stiffness force can be described by the following relationship in the whole insertion:

$$F_{\text{stiffness}} = \begin{cases} 0, & (y_{\text{tip}} < 0) \\ F(y_{\text{tip}}), & (0 \le y_{\text{tip}} \le y) \\ 0, & (y_{\text{tip}} > y) \end{cases} \tag{1}$$

here 0, y_{tip} and y refer to the location when the needle tip touches the tissue surface, the arriving location of the needle tip and the max deformation before puncture, respectively, as shown in Fig. 3.

Several polynomial models have been tried, however, third degree polynomials was found to fit best to the experiment data.

$$F_{\text{stiffness}} = d + cy + by^2 + ay^3 \tag{2}$$

here y is the deformation of tissue or the pinpoint position. The unknown a, b, c and d are constant coefficients of Eq. (2), and intercept d is assigned the value of zero for the stiffness force is zero before the needle tip getting in touch with the outer epidermis of the tissue. An inconsistent system of equation will generated as Eq. (3) when several experiment data was introduced into the Eq. (2).

$$\begin{bmatrix} y_1 & y_1^2 & y_1^3 \\ y_2 & y_2^2 & y_2^3 \\ \vdots & \vdots & \vdots \\ y_n & y_n^2 & y_n^3 \end{bmatrix} \begin{bmatrix} c \\ b \\ a \end{bmatrix} = \begin{bmatrix} F_1 \\ F_2 \\ \vdots \\ F_n \end{bmatrix} \tag{3}$$

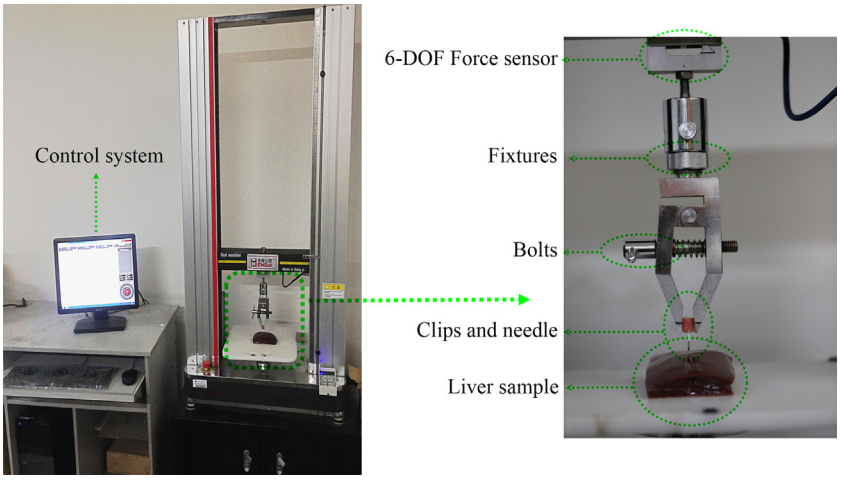

Fig. 2. HY0580 electronic universal material testing machine.

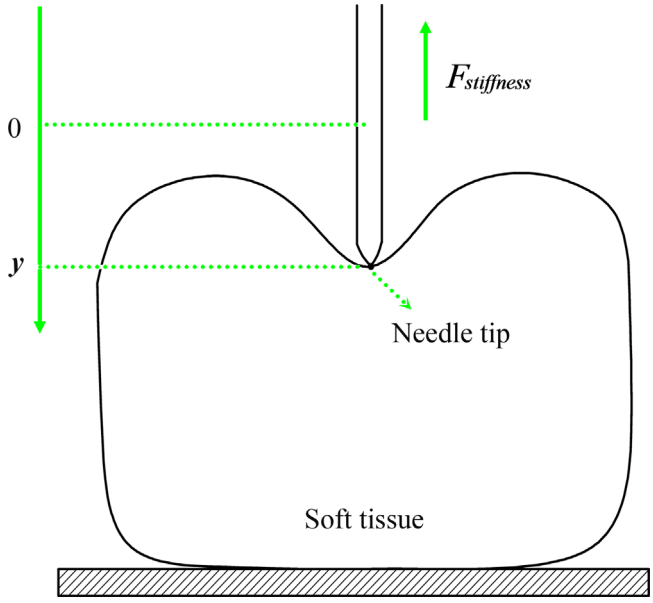

Fig. 3. Schematic diagram of the needle insertion.

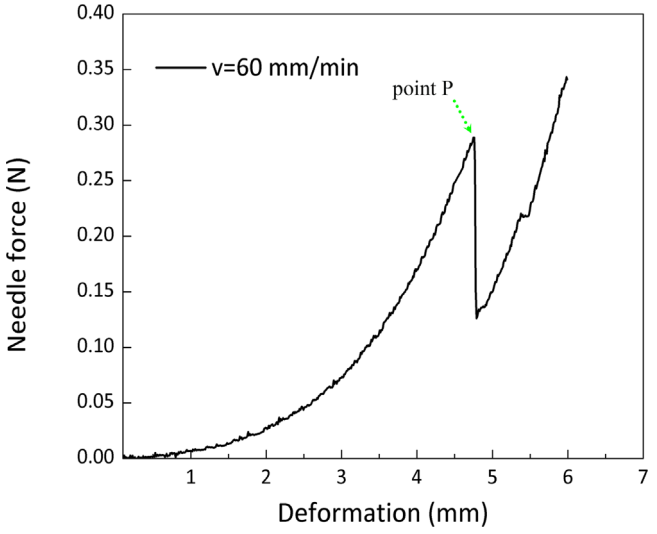

Fig. 4. A typical curve of experimental interactive forces with deformation at the insertion speed of 60 mm/min.

Simplified it as the matrix form:

$$A\,X = F \tag{4}$$

here X is the coefficient matrix, which is composed of a, b, c. A, a non-squares matrix, which is obtained when the selected data points were substituted into Eq. (2). F is the stiffness force.

The following matrix equation is normal equation of Eq. (4):

$$A^T A\overline{X} = A^T F \tag{5}$$

$$\overline{X} = (A^T A)^{-1} A^T F \tag{6}$$

here $\overline{X}$ is the least squares solution of Eq. (4).

3. Result

In the part, the interactive action between MIS suture needle and soft tissue was investigated, and the effects of velocity, besides, needle geometry, insertion angle and tissue characteristic on the puncture force were tested. All of the results below were obtained from repeated experiments.

3.1. Interactive action between suture needle and liver tissue

Fig. 4 is a typical force-deformation curve of a needle piercing into porcine liver at the velocity of 60 mm/min. There exists a overt mutation point P, we called it puncture point, which signifies a rupture happening, or in other words, the needle tip pierced the outer membrane of the liver. During the process of the needle inserting into soft tissue, the relative motion between the needle and its surrounding tissue cannot be ignored [14]. The process in the present study was divided into two phases: no rupture phase (the relative velocity is zero) and rupture phase (there exist a relative movement), as shown in Fig. 5(a) and (b).

(1) No rupture stage

As shown in Fig. 5(a), this stage occurs when the needle tip begins to touch the tissue or organ boundary, accompanied by tissue elastic deformation, and ends when the tissue boundary was breached. In this phase, the relative velocity of the needlepoint to the liver tissue was zero. The force-deformation curve segment in this stage was from zero to point P in Fig. 4. The stiffness force would reach a peak value at the time when the break happens, which was called puncture force in the present study. What is more, along with the increasing depth of the needle inserting into the liver tissue, the interaction force presented a non-linear augment, which was the stiffness force stored in the soft tissue of the surrounding contact area. Once the force surpassed a certain critical value, a distinct crack would appear suddenly in the tissue, that is to say, the needle would start to puncture the tissue [15,16]. The force–displacement curve showed a slight fluctuation feature, this was because the porcine liver tissue emerged a characterization of inhomogeneity and super viscoelasticity, and there were intensive aortic endothelial vessel and membrane lurking in the depth of the tissue (Fig. 5(c)). Consequently, when the needle tip started to contact biological tissue gradually, the continuous reaction of the inhomogeneous tissue on the needlepoint would cause the fluctuation.

(2) Rupture stage (Fig. 5(b)):

When the outer membrane was ruptured, the break stage started. During this stage, the needle tip pierced completely into the soft tissue and the puncture would be acute in the direction of insertion as the tip penetrating into the tissue (sudden crack extension). The crack continued until the strain energy levels show low enough for the crack extension. The force measured from the interaction was a resultant force of cutting force and friction force, and the relative velocity was no longer zero.

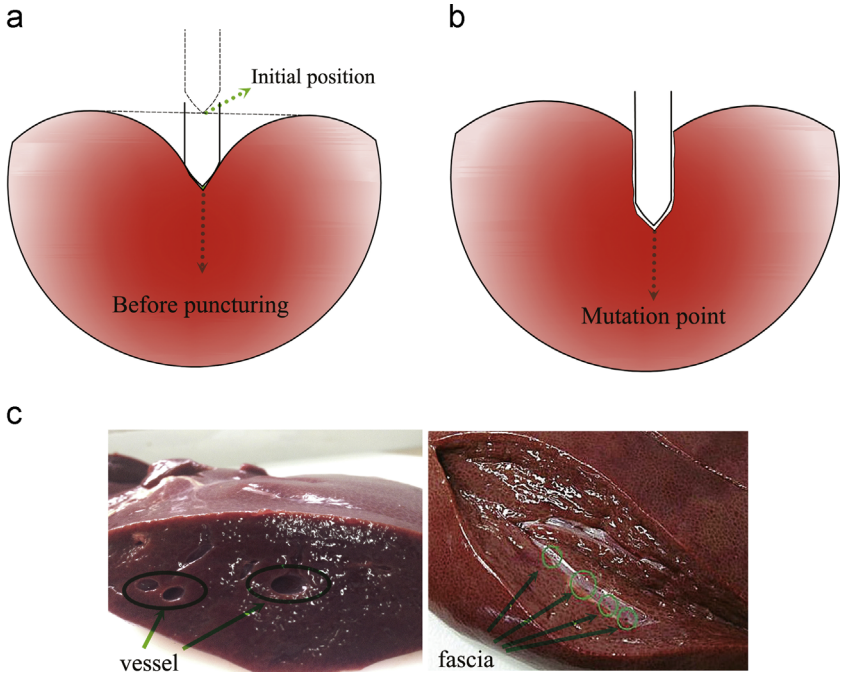

Fig. 5. The sketch map of two stages of needle insertion: (a) No rupture stage, (b) Rupture stage, and (c) The fascia and aortic endothelial vessel lurked in the depth of the liver.

3.2. Analysis of interactions model

Based on the theory of the least square method, the matrix $\overline{X}$ and the parameters a, b and c were determined, as shown in Table 1. The parameter c should tend to have a relationship with the initially approximate linear response. Parameter b seemed to be related to the lean level of the curves, the lean level was directly proportional to b. The experiment data and model predicted data with all needle types ($\Delta 1/2\ 10\times 28$, $O1/2\ 10\times 28$, $\Delta 1/2\ 8\times 20$ and $O1/2\ 8\times 20$) are demonstrated in Fig. 6. All measurements were conducted with the rate 60 mm/min. These measured points were chosen from force-deformation curves, which were truncated at the deformation where rupture starts. With least square algorithm, the RMSE (root mean squared error) for every needle type was 0.0335, 0.0313, 0.0308 and 0.0284, respectively, this showed a good fit to the experimental data. According to the experimental results, the maximum stiffness force (also the puncture force) and deformation before the first puncture event were counted. The average maximum stiffness force was about 0.2811 ± 0.0211 N, 0.2553 ± 0.022 N, 0.2311 ± 0.011 N and 0.2012 ± 0.0522 N for $\Delta 1/2\ 10\times 28$, $\Delta 1/2\ 8\times 20$, $O1/2\ 10\times 28$ and $O1/2\ 8\times 20$, respectively. The average deformation before puncturing was 5.20 ± 0.55 mm, 4.62 ± 0.23 mm, 4.02 ± 0.40 mm and 3.42 ± 0.20 mm for the above needle types, respectively.

3.3. Insertion velocity

Fig. 7 illustrates the interaction between a curved suture needle ($\Delta 1/2\ 10\times 28$) and liver tissue at different insertion velocities. The typical variations of total force with

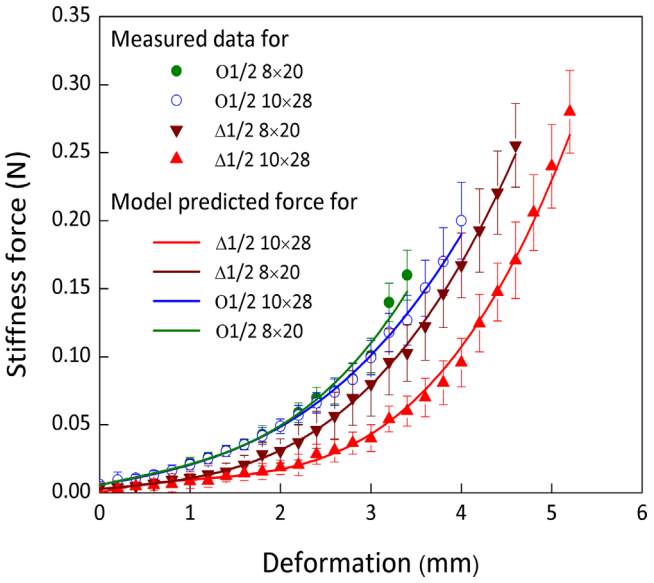

Fig. 6. Comparison between predicted force model and the experimental stiffness force with $\Delta 1/2\ 10\times 28$, $\Delta 1/2\ 8\times 20$, $O1/2\ 10\times 28$ and $O1/2\ 8\times 20$.

deformation at ten different velocities are shown in Fig. 7(a). The colorful imaginary straight line vividly expressed the tangent of the force–displacement curve in the initial position. An obvious trend showed the slope increased remarkably by a factor of the increasing insertion velocity, which was from 30 mm/min to 120 mm/min. However, the trend was unconspicuous when the speed was up to 100 mm/min, and the slope tended to be constant. It also pointed that the stiffness force strengthened with velocity speeding up. To have a further and clear understanding of the impact of the insertion speed on the puncture force, a repetitive testing had been performed, the

Table 1
The determined values of parameter c, b and a with four needle types.

		Needle types			
		Δ1/2 10 × 28	Δ1/2 8 × 20	O1/2 10 × 28	O1/2 8 × 20
Coefficient	c (N/mm)	0.0822	0.0349	0.0199	0.0154
	b (N/mm^2)	−0.2151	−0.0909	−0.0221	−0.0211
	a (N/mm^3)	0.1911	0.0854	0.0081	0.0191

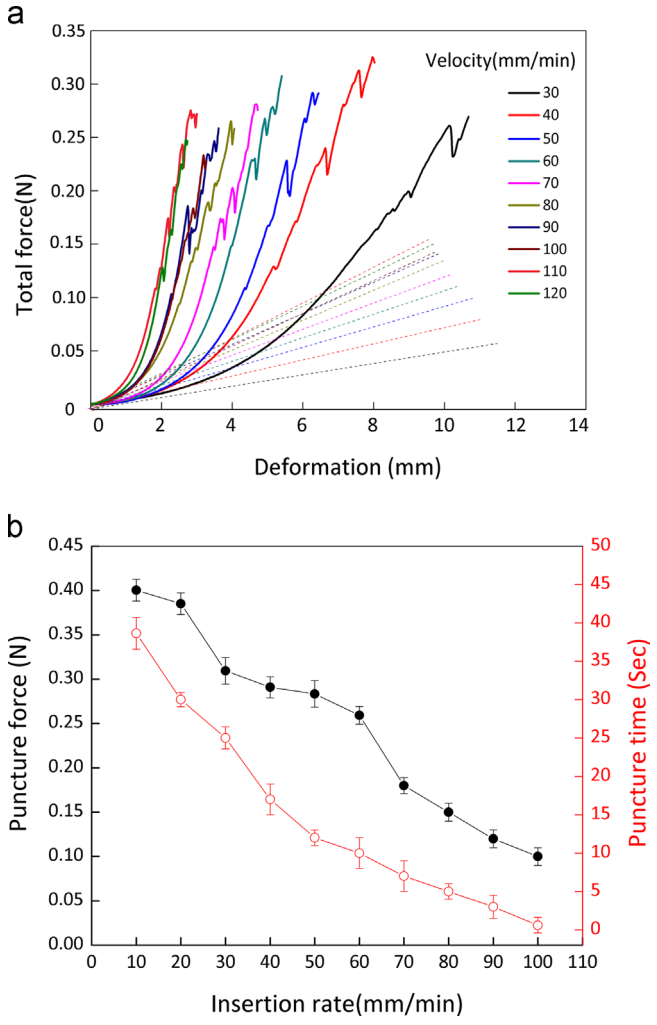

Fig. 7. The interaction between a curved suture needle (Δ1/2 10 × 28) and liver tissue, (a) Typical variations of total force with deformation at various velocities, the colorful imaginary straight line vividly expressed the tangent of the force–displacement curves in the initial position, (b) A statistic graph about the rough relationship of insertion speed-puncture force and insertion speed-the time for the first puncture, repetitions for ten times.

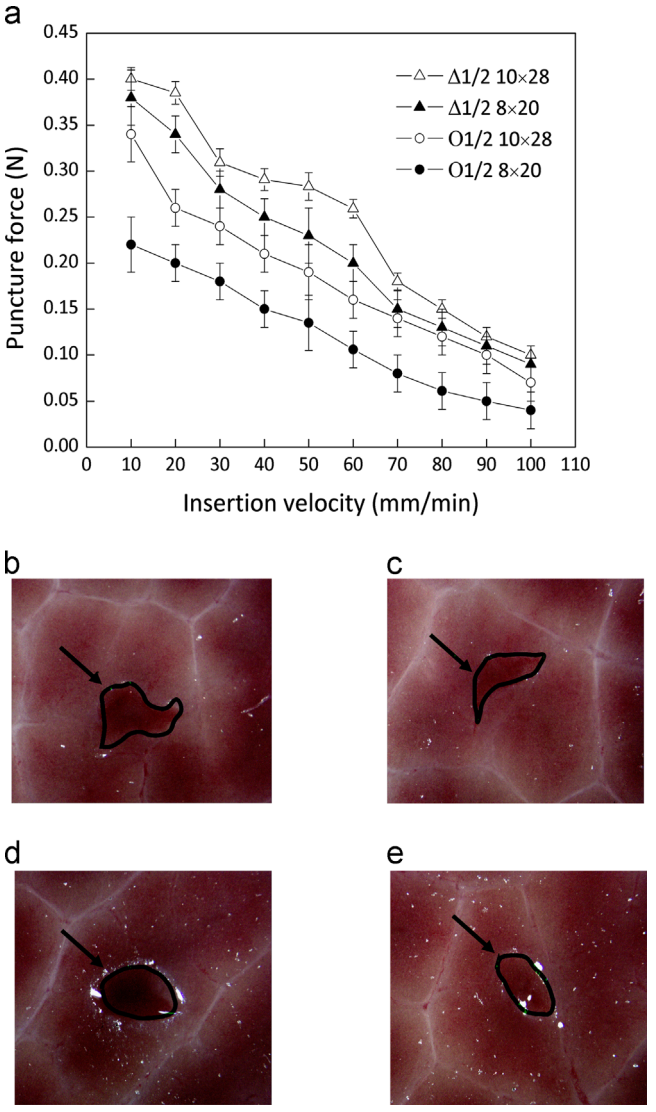

Fig. 8. Comparison of puncture force and crack morphology with fourfold magnifications for different types of needle. (a) Average puncture force on the conditions of different needle geometries and insertion velocities, (b) Δ1/2 10 × 28, (c) Δ1/2 8 × 20, (d) O1/2 10 × 28, (e) O1/2 8 × 20.

repetitions for every parameter are ten times. The parameter of velocity set here was from 10 mm/min to 100 mm/min, and the rough relationship between puncture force and insertion speed was shown in Fig. 7(b). It was obvious that puncture force and the time for the first puncture seemed to be lessened significantly with the increasing injection velocity, which was similar to the study [8].

3.4. Needle geometries

Fig. 8(a) illustrates the impact of needle geometries showed in Fig. 1(a) on the puncture force during the process of insertion. The insertion velocity was from 10 mm/min to 100 mm/min. From the horizontal comparison, the average

puncture force decreased remarkably with the increasing inject speeds for the same needle geometry, which further confirmed the reliability of the conclusion mentioned in Section 3.1. From the longitudinal comparison, the average puncture force with the needle tip of triangle cross-section showed larger than that of round cross-section at the same needle size and speed. Furthermore, at the same needle cross-section shape and speed, the puncture force came from the needle size of 10×28 was larger than that of 8×20. The results indicated that the needle with the triangle cross-section and larger size increased the puncture force.

The crack morphology of pig liver caused by the needle tip were found to be affected by the needle geometry. Fig. 8(b)–(e) shows the typical crack appearance in pig liver inserted by different needle geometries with fourfold magnifications. The triangular cross-section tip usually generated an irregular shaped crack, while the circular one was diametrical, which was approximately an ellipse. The irregular shape was attributed mostly to the continuous cutting caused by the nipping edge of the triangular needle, and the crack propagation would be bad for tissue repairing. On the contrary, due to the smooth surface, no obvious crack growth was exposed after inserting by the circular cross-section tip needle.

3.5. Insertion angle

Fig. 9 shows the influence of insertion angle (45°, 60°, 75° and 90°) on the puncture force for four needle types. The same insertion velocity is 60 mm/min. For the same needle, the mean penetration force significantly decreased with the increasing insertion angle, and the force reaches the lowest value when the angle was 90° (the needle stabs vertically into tissue surface).

3.6. Influence of tissue characteristics

In order to determine the effect of tissue characteristics on the insertion force, the other four types of tissues were tested with suture needle Δ1/2 10×28 and the insertion speed was 60 mm/min. Fig. 10(a) and (b) illustrate the typical insertion forces with time for five different tissues, the curves of porcine liver and rabbit liver show several times mutation, but only one for other tissues. It can be owing to the common characteristics of liver structure: intricate vein and membrane lurked in the depth of liver. Fig. 10(c) shows the relationship among puncture force, needle types and tissue types, Table 2 lists the specific data. Obviously, the puncture force of pig skin surpassed greatly than that of other tissues, and the puncture force was almost several-fold than porcine liver. For the organs of rabbit, the puncture forces of both small and large intestine were about 10 times as much as the liver. The puncture times were diverse due to the differences in tissue structure. The time for porcine skin, porcine liver, rabbit small intestine, rabbit larger intestine, rabbit liver was 11.22 ± 1.44 s, 7.31 ± 0.93 s, 16.81 ± 2.14 s, 22.05 ± 3.12 s, 7.23 ± 1.22 s, respectively. By comparison, the puncture time of both pig liver and rabbit liver

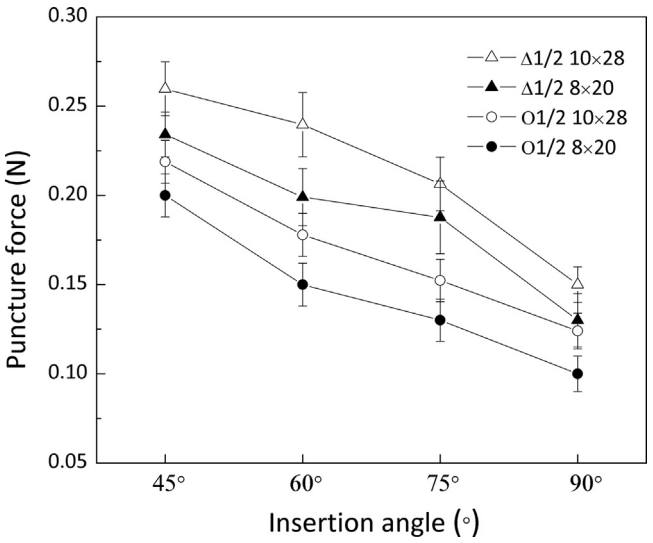

Fig. 9. Mean puncture force under the different insertion angles and needle types.

was the shortest, which meant that they were relatively easy to be punctured.

4. Discussion

According to previous studies, little current data is available about the influence of insertion velocity on the puncture force. Frick et al. [17] investigated the influence of velocity on insertion force with a straight (0.88 mm) suture needle inserting into sheep skin, but no significant effect of velocity on axial force was found. However, the completely different results were obtained in the present study. The viscoelastic response of liver strongly depended on the velocity. The liver showed more noticeable stiffness characteristic under higher insertion velocity (Fig. 7), that meant the viscoelastic response of liver weakened with the increasing velocity, as a result, the tissue was more easily punctured. That meant the puncture force and time decreased with the increasing injection velocity.

The needle geometry had important impact on the puncture force in the insertion process. The results indicated that the needle with the triangle cross-section and larger diameter increase the puncture force, which can be attributed to the triangle one and large diameter process the larger cross section, and then the larger resistance the needle tip experience. The result can assist to optimize needle design and provide better tips for the medical practitioner when they are confused about what needle types to choose.

Because biological tissue is typically inhomogeneous and anisotropic, the mechanical properties depend on position and orientation. Therefore, it is important to consider the location where the needle is inserted, as well as the direction of needle insertion. Crouch et al. [6], Howard et al. [18] and Langevin et al. [19] inserted their needles perpendicular into the tissue surface. Okuno et al. [20] and Hiemenz et al. [21] investigated needle insertions from other angles. The results in the present study showed that the penetration force reduced when the

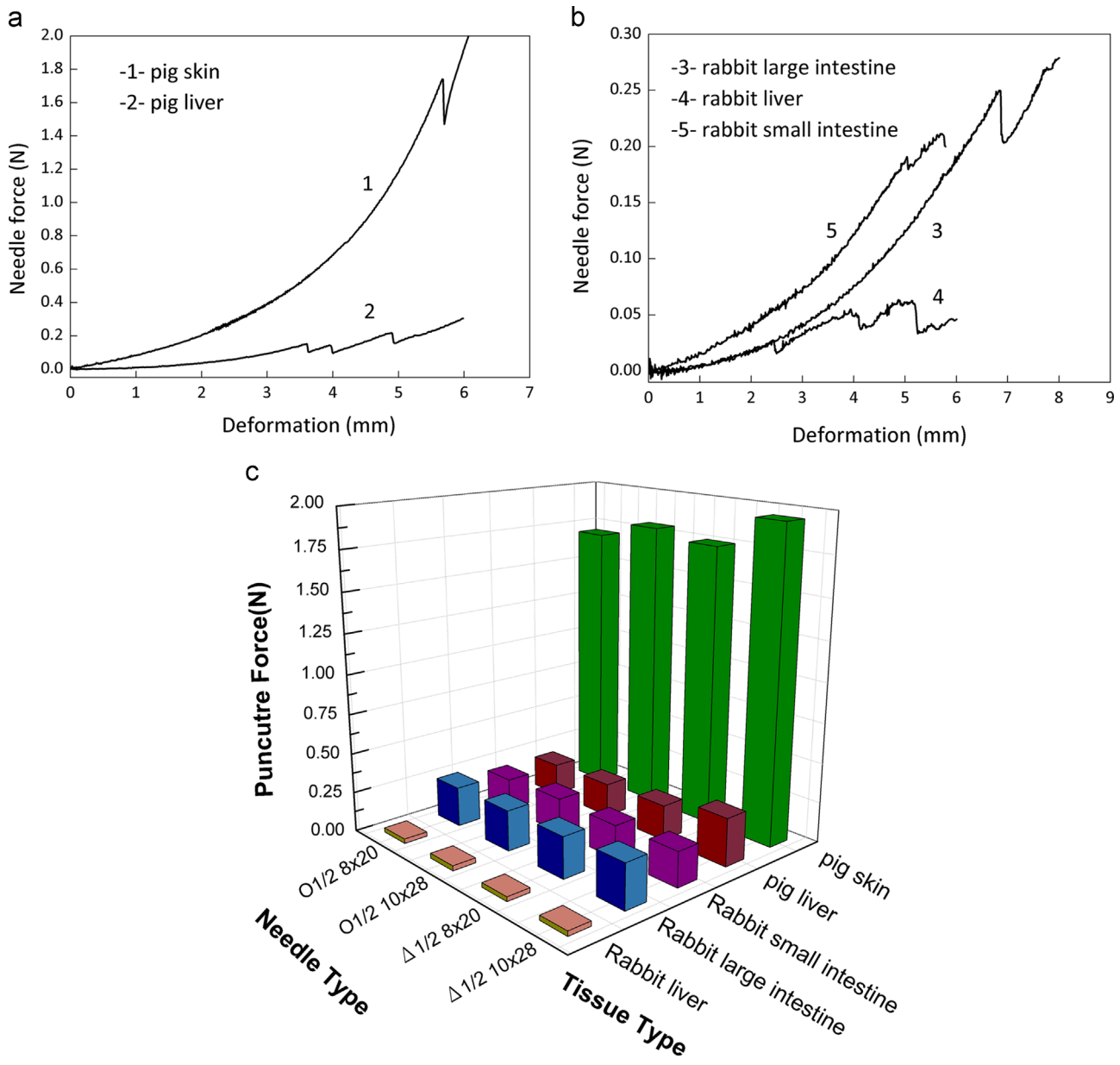

Fig. 10. The typical insertion forces with time for five different tissues (Δ10 × 28 needle, $v = 70$ mm/min), (a) Porcine skin and liver, (b) Rabbit liver, rabbit small and large intestine, and (c) Three dimensional histogram of the relationship among puncture force, needle types and tissue types.

Table 2
The specific puncture force with five tissue types and four needle types.

	Needle types			
	O1/2 8 × 20	O1/2 10 × 28	Δ1/2 8 × 20	Δ1/2 10 × 28
Rabbit liver	0.028	0.030	0.029	0.033
Rabbit large intestine	0.251	0.255	0.272	0.282
Rabbit small intestine	0.201	0.221	0.203	0.238
Pig liver	0.222	0.215	0.223	0.310
Pig skin	1.715	1.802	1.753	1.950

insertion angles changed from 45° to 90°, as the resistance was larger with the increasing of angle. The insertion angle is defined by the intersection angle between tangent of the needle curve and the tissue surface. The control of insertion angle is implemented by prior calibration. When a surgeon drives a needle through tissue during suturing, the research of insertion angle can be a good reference for him or her, which can enhance the efficiency of suture in MIS and offer the learner a formal suture training skill.

Fig. 10(c) illustrates porcine skin shows larger puncture force than other tissues with the same needle, it was decided by the hardness and thickness of the porcine skin. The brittleness

was obviously higher than others, as a result, the rabbit liver, showed smaller puncture force, the pig liver, rabbit large and small intestine have a similar stiffness characteristic. The elastic modulus may be a significant reference to explain the huge difference in the mechanical properties of the above samples, here we just summarize the puncture force trend, consequently, the elastic modulus will be the further work.

In this paper, all the influence factors were considered independently, multivariate analysis should be premeditated to find more indications. Moreover, due to a stupendous disparity between the experimental condition and the real clinic operation, characterizing the suture action in vivo clearly is in troubled water, whether the measurement ex vivo can be a substitute for in vivo measurement or not. Consequently, the question needs a further examination in the future work. What is more, we do not clearly know if the trends we found above were analogous to all various soft tissues, or there exists a huge quantitative disparity among them. While these verdicts are just from limited times of tests, plenty of experiments need to be conducted, and a reliable theoretical model should be established to verify its veracity.

5. Conclusion

In this study, the interactive action between MIS suture needle and soft tissue was investigated to simulate the real surgical suture needle-tissue operation conditions. The purposes were to reveal the mechanism of interactive action during the process of the needle inserting into soft tissue, and to study the effects of different insertion velocities, needle geometries, insertion angles and tissue characteristics on the puncture force. These factors affecting the puncture force can be considered to model suture needle-tissue interaction. Experimental results demonstrated that the process of insertion was divided into two phases: no rupture phase and rupture phase. No rupture stage is a deformation event that starts at 0 mm and continues until a deformation at which the needle stiffness force reaches its maximum, and the stiffness force is the only force. Rupture stage is relatively a complicated process along with crack propagates in the body in response to the needle displacement, the main force are friction force and cutting force. The puncture force generated at the mutation point where the tissue boundary was breached. The puncture force and time for the first puncture significantly decreased with the rising injection velocity. The needle geometry had important influence on the puncture force. The needle with triangle cross-section tip and larger size showed higher puncture force than that of round cross-section and smaller one. The penetration force reduced evidently with the increasing insertion angle, and it reached the lowest value when the needle was perpendicular to the tissue surface. Due to the differences among tissue structures and the mechanical properties, the puncture force and time were diverse for the different tissues. Moreover, the non- linear least squares algorithm was used to develop an empirical single-parameter model of third-degree polynomial which could predict the stiffness force when a suture needle inserted into a complex liver tissue.

Ethical approval

All the work was carried out in accordance with my institution guidelines and in accordance with the EU Directive 2010/63/EU.

Acknowledgments

This work was supported by National Natural Science Foundation of China (No. 51290291).

References

[1] Y. Wang, R.K. Chen, B.L. Tai, K. Xu, Study of insertion force and deformation for suturing with precurved NiTi guidewire, J. Biomech. Eng. 5 (2015) 137.
[2] R.C. Jackson, M.C. Cavusoglu, Modeling of needle-tissue interaction forces during surgical suturing, in: Proceeding of 2012 IEEE International Conference on Robotics and Automation, Minnesota, USA, 2012.
[3] A.M. Okamura, C. Simone, M.D. O'Leary, Force modeling for needle insertion into soft tissue, IEEE Trans. Biomed. Eng. 51 (2004) 1707–1716.
[4] T.K. Podder, J. Sherman, E.M. Messing, D.J. Rubens, D. Fuller, J.G. Strang, R.A. Brasacchio, Y. Yu, Needle insertion force estimation model using procedure-specific and patient-specific criteria, in: Proceeding of the 28th Annual International Conference of the IEEE Engineering in Medicine and Biology Society, New jersey, USA, 2006.
[5] S.P. DiMaio, S.E. Salcudean, Needle insertion modeling and simulation, IEEE Trans. Robot. Autom. 19 (2003) 2098–2105.
[6] J.R. Crouch, C.M. Schneider, J. Wainer, A.M. Okamura, A velocity-dependent model for needle insertion in soft tissue, in: Proceeding of the 8th International Conference on Medical Image Computing and Computer-assisted Intervention, Palm Springs, USA, 2005.
[7] M. Mahvash, P.E. Dupont, Fast needle insertion to minimize tissue deformation and damage, in: Proceeding of the 2009 IEEE International Conference on Robotics and Automation, Kobe, Japan, 2009.
[8] M. Mahvash, P.E. Dupont, Mechanics of dynamic needle insertion into a biological material, IEEE Trans. Biomed. Eng. 57 (2010) 934–943.
[9] N. Chentanez, R. Alterovitz, D. Ritchie, L. Cho, K.K. Hauser, K. Golderg, J.R. Shewchuk, J.F. O'Brien, Interactive simulation of surgical needle insertion and steering, ACM SIGGRAPH 88 (2009) 1–10.
[10] S. Misra, K. Reed, B. Schafer, K. Ramesh, A. Okamura, Observations and models for needle-tissue interactions, in: Proceeding of the 31th Annual International Conference of the IEEE Engineering in Medicine and Biology Society, Atlanta, USA, 2009.
[11] P. Yu, W. Li, W. Sun, The study on mechanical differences of the hepatic portal vein between the human and pig, Chin. J. Clin. Anat. 5 (2004) 95–97.
[12] Y.C. Fung, R. Skalak, Biomechanics: mechanical properties of living tissues, J. Appl. Mech. 2 (1982) 464–465.
[13] M. Ottensmeyer, J.K. Salisbury, Jr., In vivo data acquisition instrument for solid organ mechanical property measurement, in: Proceeding of the Conference on Medical Image Computing and Computer-Assisted Intervention, Utrecht, the Netherlands, 2001.
[14] D.J. van Gerwen, J. Dankelman, J.J. vanden Dobbelsteen, Needle-tissue interaction forces – a survey of experimental data, J. Med. Eng. Phys. 34 (2012) 665–680.
[15] Y. Kobayashi, T. Sato, M.G. Fujie, Modeling of friction force based on felative velocity between liver tissue and needle for needle insertion simulation, in: Proceeding of the 31th Annual International Conference of the IEEE Engineering in Medicine and Biology Society, Atlanta, USA, 2009.
[16] L. Barbe, B. Bayle, M. de Mathelin, A. Gangi, Needle insertions modeling: identifiability and limitations, Biomed. Sig. Process. Control 2 (2007) 191–198.

[17] T.B. Frick, D.D. Marucci, J.A. Cartmill, C.J. Martin, W.R. Walsh, Resistance forces acting on suture needles, J. Biomech. 34 (2001) 1335–1340.

[18] M.A. Howard, B.A. Abkes, M.C. Ollendieck, M.D. Noh, R.C. Ritter, G. T. Gillies, Measurement of the force required to move a neurosurgical probe through in vivo human brain tissue, IEEE Trans. Biomed. Eng. 46 (1999) 891–894.

[19] H.M. Langevin, D.L. Churchill, J.R. Fox, G.J. Badger, B.S. Garra, M. H. Krag, Biomechanical response to acupuncture needling in humans, J. Appl. Physiol. 91 (2001) 2471–2478.

[20] D. Okuno, T. Togawa, H. Saito, K. Tsuchiya, Development of an automatic blood sampling system: control of the puncturing needle by measuring forces, in: Proceedings of the 20th Annual International Conference of the IEEE Engineering in Medicine and Biology Society, Hong Kong, China, 1998.

[21] L. Hiemenz, D. Stredney, P. Schmalbrock, Development of the force-feedback model for an epidural needle insertion stimulator, J. Stud. Health Technol. Inform. 50 (1998) 272–277.